SELECTIVE ELECTROCHEMICAL REDUCTION OF CO_2 TO HIGH VALUE CHEMICALS

Grant agreement no.: 851441

***Start date**: 01.01.2020 – **Duration**: 36 months*

***Project Coordinator**: Dr. Brian Seger - DTU*

DELIVERABLE REPORT

4.2 REPORT ON IN-SITU OBSERVATIONS OF CATALYST STRUCTURE AND LOCALIZED ACTIVITY USING ELECTROCHEMICAL AFM SYSTEM		
Due Date	30-6-2021	
Author (s)	Thomas Burdyny; Erdem Irtem; Mengran Li	
Workpackage	4	
Workpackage Leader	Thomas Burdyny	
Lead Beneficiary	TUD	
Date released by WP leader	28-06-2021	
Date released by Coordinator	28-06-2021	
DISSEMINATION LEVEL		
PU	*Public*	***X***
PP	*Restricted to other programme participants (including the Commission Services)*	
RE	*Restricted to a group specified by the consortium (including the Commission Services)*	
CO	*Confidential, only for members of the consortium (including the Commission Services)*	
NATURE OF THE DELIVERABLE		
R	*Report*	***X***
P	*Prototype*	
D	*Demonstrator*	
O	*Other*	

SUMMARY	
Keywords	Electrochemical CO_2 reduction; atomic force microscopy; catalyst structure;
Abstract	The Cu catalyst undergoes dynamic structural changes during the electrochemical CO_2 reduction (ECO2R), and such structural change could profoundly impact the cathode activity and long-term stability. Recent operando studies focus on a planar electrode immersed in the electrolyte with limited current densities < 10 mA cm^{-2}, but the findings are challenging to understand the catalyst behavior in a gas-diffusion electrode that can operate at above 100 mA cm^{-2}. This deliverable investigates the structural evolution of the Cu catalyst in a configuration of GDE during ECO2R catalysis at current densities up to 200 mA cm^{-2} by using the operando electrochemical atomic force microscope (EC-AFM). We find that the Cu catalyst restructuring takes place via (1) an increase of surface roughness likely due to the electroreduction of nature oxidized Cu species at the surface and (2) surface flattening and formation of nanocuboids Cu (100) facets, particularly at high current densities beyond 100 mA cm^{-2}. Both processes contribute to the promotion of ethylene production but a different extent. We believe the catalyst surface restructuring is not the dominant factor determining the cathode performance at high current density. The conclusion from these results suggests new directions for the design of the Cu catalyst structure of the GDE to further improve the ECO2R reactivity and stability.
Public abstract for confidential deliverables	

REVISIONS			
Version	**Date**	**Changed by**	**Comments**
0.1	28-06-2021	Aaron Li	

REPORT ON THE IMPACT OF REACTION INTERMEDIATE ON ECO2R SELECTIVITY TOWARDS ETHYLENE

CONTENT

1 INTRODUCTION

This deliverable report describes the experimental and analytical approach based on an electrochemical atomic force microscope (EC-AFM) to in situ investigate the topographical change of the Cu catalyst layer deposited on a gas-diffusion layer (GDL) during and after electrochemical CO_2 reduction (ECO2R). Specifically, this report investigates the structural evolution of the Cu catalyst layer on Freudenberg GDL under various constant current densities between 10 mA cm^{-2} and 200 mA cm^{-2} in a gas-diffusion electrolysis system.

Scientific background:
Recent studies have reported that copper catalysts undergo a dynamic change in their morphology during the ECO2R at low current densities (<10 mA cm^{-2}). In most of these experiments, the Cu catalysts such as polycrystalline Cu foil[1] and Cu nanoparticles[2-3] were usually immersed in a CO_2-saturated electrolyte such as $KHCO_3$ aqueous solution. The conclusions from these recent findings are as below:

General observations:

- The polycrystalline Cu foil tends to restructure to (100) facets under cathodic potentials in the presence or absence of CO_2;[1, 4-5]
- The Cu catalyst surface becomes rough during ECO2R;[3, 6]
- The Cu nanocube catalyst loses its cubicity under ECO2R operating conditions.[3]

Reported critical factors for the restructuring process:

- The oxidation state of the Cu: oxidized Cu catalyst show a significant restructuring process at ECO2R;[5, 7]
- The applied cathodic potential: more negative potential intensify the restructuring process;[3]
- Surface intermediate coverage: H and CO adsorbate could stabilize the (111) and (110) facets.[3]

However, the insights generated from this approach are very limited for understanding the catalyst restructuring process over a gas diffusion electrode (GDE). Most of these studies used flat electrodes that are completely immersed in the electrolyte. The flat electrode has limited active sites, and the diffusion of the gas reactant and products occurs between electrode and electrolyte. This setup is different from the GDE, which has a high density of active sites in the catalyst layer and allows the transport of gaseous reactant and products between the catalyst and gas chambers. (see **Figure 1**) Very recently, Nesbitt and Smith[8] successfully developed a cell at TUD for the EC-AFM to in-situ study the catalyst's structural changes over a silver GDE during ECO2R at up to 100 mA cm^{-2}. Hence, we continued to use a similar cell set up to study the structural evolution of the Cu catalyst structure under varied current densities up to 200 mA cm^{-2} over a GDE configuration.

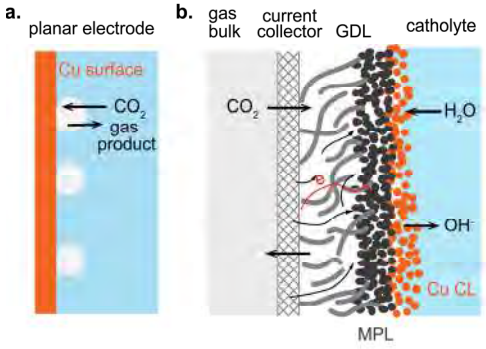

Figure 1: A schematic of (a) the planar electrode immersed in the electrolyte and (b) the gas-diffusion electrode located at the interface between gas and electrolyte.

2 SCOPE

This deliverable contributes to WP4 (ethylene production) by providing qualitative and quantitative information on the local structural evolution of the Cu catalyst layer on a GDL during ECO2R at high current densities. Our task is to identify the role of the cathode potential (or current densities) in the dynamic surface restructuring of the catalyst layer of a GDE and the potential link between the catalyst structure and cathode performance when paired with gas chromatography data.

The configuration of the EC-AFM cell used in this deliverable is restricted to one chamber electrolysis cell with the presence of static electrolyte and flowing CO_2 . A stagnant electrolyte was chosen to prevent disruption of the AFM probe and signal. The reactivity and product selectivity of the GDE was only measured in a flow cell with a flowing catholyte and CO_2. The current densities for the EC-AFM cell are up to 200 mA cm^{-2}, which is close to the operation conditions of a flow cell. This work is limited to the Freudenberg GDL because this GDL could provide a flat and uniform catalyst layer, which is vital for high-quality AFM characterization.

3 RESULTS AND DISCUSSION

This section presents the experimental description, results, and discussion for the GDE performance evaluation and operando EC-AFM measurements. All the experiments are tested under constant current densities. The GDE is composed of a nominal thickness 150 nm sputtered Cu catalyst layer and a Freudenberg GDL.

Freudenberg-type GDL enables a smooth catalyst surface due to its tightly packed carbon fibers in the backbone. The highly porous layer (HPL), as shown in **Figure 2**, is facing the CO_2 gas chamber, with a 15-40 micron pore opening and carbon fibers that are eight microns in diameter. **Figure 2**b presents the scanning electron micrographs (SEM) of the top microporous layer (MPL) of the pristine GDL, and **Figure 2**c shows the 150 nm thick sputtered Cu layer. The MPL is made up of carbon nanoparticles (~50 nm) and PTFE binders and serves as current collectors to distribute electrons, gas-transport pathways for gas diffusion, and support for the catalyst layer. Only a few cracks were found with less than a micron in width and a hundred micron in length. Nevertheless, this flat GDL substrate supports a compact Cu layer (Figure 1c) with a particle size ranging from 80 to 170 nm in diameter.

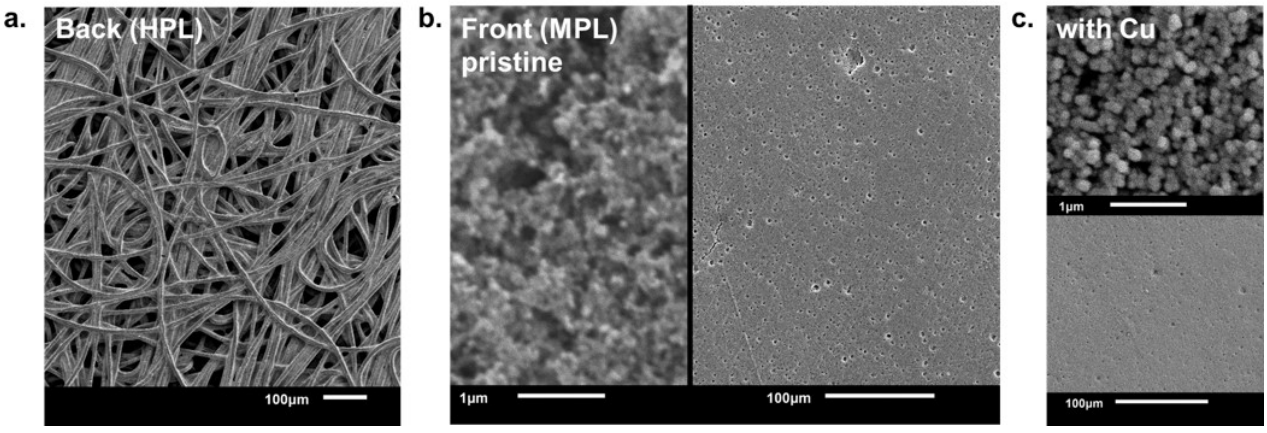

Figure 2: SEM images of Freudenberg type gas diffusion layers showing **a)** high porous backside of the substrate **b)** microporous layer at the front side with carbon nanoparticles of the pristine substrate, **c)** after sputtering of 150 nm thick copper layer.

3.1 GDE performance evaluation in the flow cell

An electrochemical flow cell reactor, with details described in the Deliverable 4.1 report, was used to test the ECO2R performance of the GDE sample. We used the Ni mesh as the anode and Ag|AgCl (saturated KCl) as the reference electrode. As the EC-AFM cell requires the presence of an electrolyte, the flow cell was fed with a flowing 1M $KHCO_3$

aqueous solution as the catholyte and 1M KOH aqueous solution as the anolyte. Both electrolytes were circulated at a flow rate of 20 mL min^{-1}. A mass flow controller also supplied the CO_2 gas to the cathode gas chamber at a flow rate of 20 sccm. A Nafion 117 cation-exchange membrane separated the cathode and anode chamber. A gas chromatogram analyzed the gas effluent of the reactor. Constant current tests were conducted between 50 – 300 mA cm^{-2}, and each point was tested for a minimum of 1200 s.

Figure 3 shows the results of the selectivity and activity performance of the GDE. Ethylene (C_2H_4) is the most selective gaseous product at current densities higher than 100 mA cm^{-2}, with a peak faradic efficiency (FE) of 41.2 % at 300 mA cm^{-2}. The drop of CO FE corresponds well with the statement in the literature that CO-CO coupling is a sink for ethylene production. However, the limited total ECO2R selectivity could be related to the competitive hydrogen evolution reaction in the pH-neutral bicarbonate electrolyte and insufficient CO_2 supply at high current densities. **Figure 3**b shows the catalyst activity in terms of partial current density. The iR-corrected potential of the GDE changed from -1.36 to -1.8 V vs. Ag/AgCl when the current applied increased from 50 to 300 mA cm^{-2}. Propane and ethylene demonstrated a similar trend, in contrast to CO and methane (CH_4), which indicates that the selectivity of these compounds could be controlled by a different rate-determining step. The increase of C_2H_4 selectivity with the current densities could be related to the increased local pH and catalyst morphology. The latter will be investigated in detail, mainly using the EC-AFM in this deliverable report.

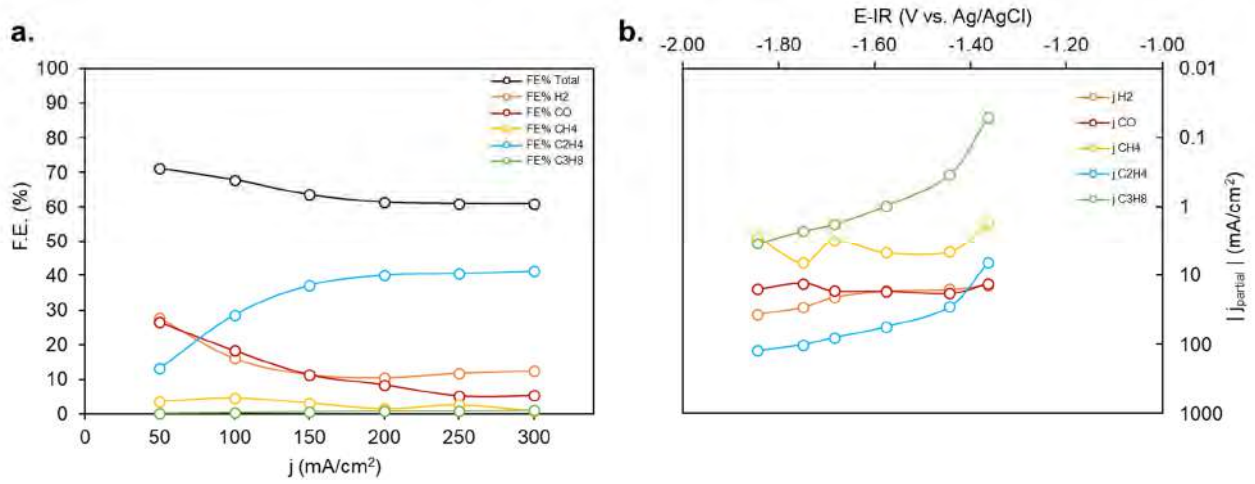

Figure 3: a) Faradaic efficiency and **b)** partial current density results of the electrochemical CO_2 reduction tests, conducted with GDE in a flow cell configuration at 20 sccm gas flow rate, circulating 1M $KHCO_3$ and KOH for catholyte and anolyte, respectively.

3.2 GDE activity evaluation in the EC-AFM cell

We also investigated the reactivity of the GDE in a cell, as illustrated in **Figure 4**a and b. The electrode was placed on top of a current collector such as Cu or Al foil, and was sealed by a tape with a hole that allows the exposure of the Cu catalyst layer to the 1M $KHCO_3$ aqueous electrolyte. There is also a hole underneath the GDE to allow the diffusion of gaseous CO_2 and products between the gas chamber and the catalyst layer. The CO_2 gas was fed into the cell through the gas chamber at a flow rate of 1 mL min^{-1} by a syringe pump. A platinum wire served as an anode and was immersed in the aqueous electrolyte. A Bruker Dimension Icon EC-AFM equipped with ScanAsyst Fluid or Fluid+ cantilever was used for the operando morphological measurement. (see **Figure 4**c and d)

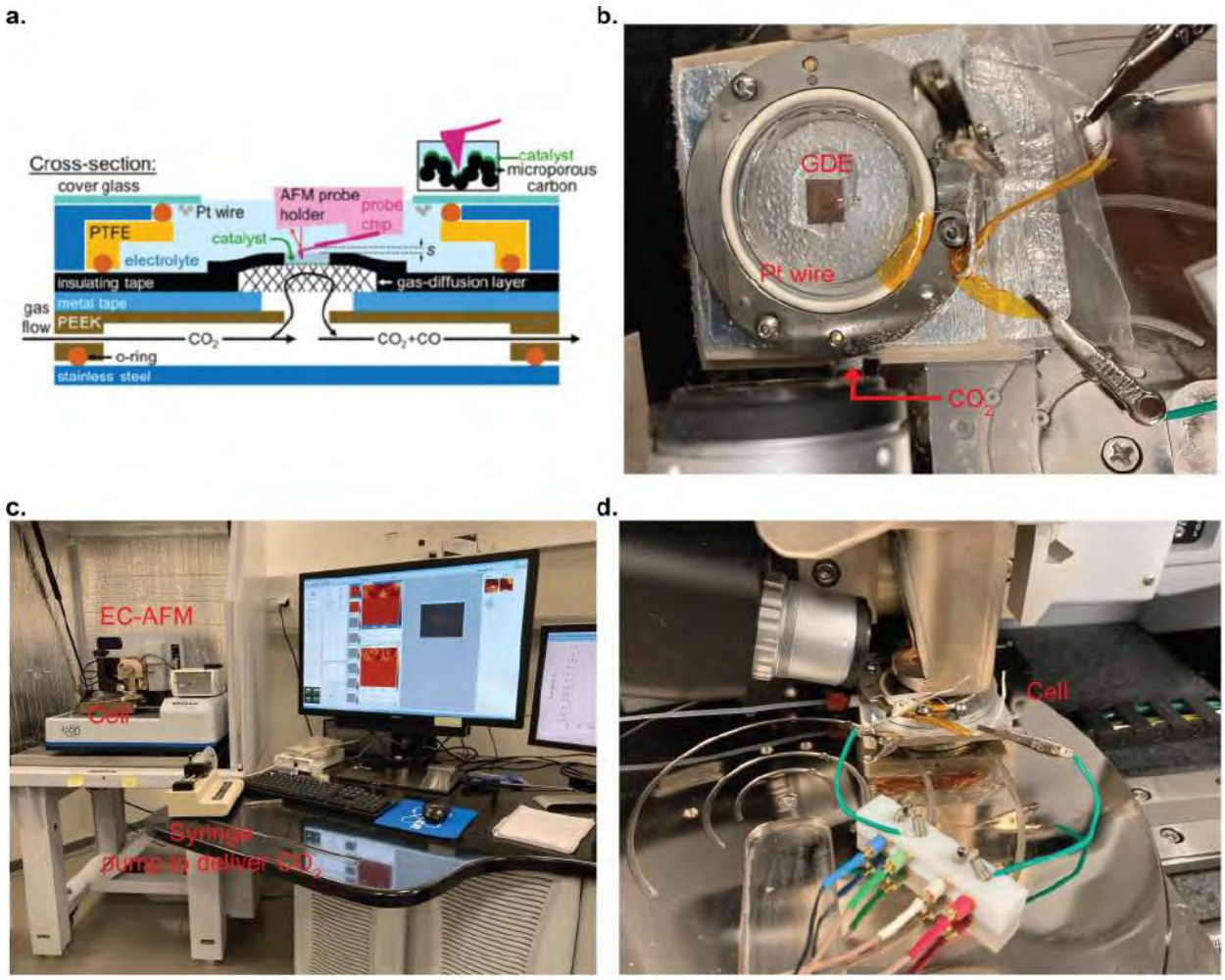

Figure 4: a) A schematic illustration of the EC-AFM cell and its operation during EC-AFM characterization, cited from ref [8]. Photos of **b)** the EC-AFM cell, **c)** the EC-AFM system, and **d)** the cell connected with the potentiostat probe when the AFM tip was engaging with the catalyst layer in the electrolyte.

Before the operando EC-AFM test, we studied the relation between the current densities and applied cell/cathode potentials. The cell was tested at constant current densities for 30 s from 0 to 200 mA cm^{-2} in either two- (see **Figure 5**a) or three-electrode (see **Figure 5**c) configuration. We also recorded a video of the cell during the electrochemical treatment to study its response to the applied potential. **Figure 5**b shows a few selected frames of the video. The color of the Cu catalyst transformed from dark orange to orange-red (the color of the metallic Cu), particularly at current densities over 50 mA cm^{-2}. This catalyst color transition during ECO2R suggests that the natural Cu oxide layer of the catalyst was slowly reduced to metallic Cu during ECO2R. This result is consistent with the Pourbaix diagram of Cu and the reported findings by Lee et al.[4] and Li et al. [9].

In the three-electrode electrochemical study, we placed a micro Ag|AgCl reference electrode close to the catalyst in the electrolyte (see the inset photo of **Figure 5**c) and applied the same constant current densities to the cell. The relation of the current densities and applied cathode potentials vs. Ag|AgCl is shown in **Figure 5**c. **Figure 5**d compares the correlation of current densities with the cell potential and applied cathode potential. The cathode potential is similar to the cathode potential recorded in the flow cell test. (see **Figure 3**b)

Interestingly, we observed disruption of the electrochemical signal at 50 mA cm^{-2} in both tests. The recorded cell potential mainly consists of cathode potential, anode potential, and ohmic potential loss in electrolytes between the electrodes. The recorded applied cell potential is primarily composed of cathode potential, and the

uncompensated resistance originated from the ohmic resistance between the cathode and the reference electrode. The disruptions of the recorded signals could result from the formation of appreciable bubbles at the electrode surface. These bubbles may lead to a loss of electrochemically active sites and an increase of ohmic resistances in between the electrodes.

We applied the electrochemical impedance spectroscopy at OCV to identify the ohmic resistance of the cell (46.70 Ω cm^2) and the uncompensated resistance (3.79 Ω cm^2), see **Figure 5**e. We also calculated the iR-corrected cathode potential vs. the reversible hydrogen electrode (RHE), and its relationship with the current densities is shown in **Figure 5**f. However, the reference electrode may interfere with the operation of the EC-AFM, so the EC-AFM cell operated in the configuration of two electrodes. The chronopotentiometry curves of the cell during the AFM characterization are shown in **Figure 5**g. At low current densities, including 10, 20, 30 mA cm^{-2}, we recorded the topography of the catalyst layer during the ECO2R process. The electrochemical conditioning duration usually lasted for more than 1000 s. However, a current density higher than 50 mA cm^{-2} significantly disrupted the AFM probe and led to poor quality of the AFM images. To resolve this critical issue, we tried to take the AFM image at the exact location of the catalyst right after cathodic conditioning for 5 min. Most of the cell potentials instead of the case of 30 mA cm^{-2} are consistent with the ex-situ cell measurement shown in **Figure 5**a. This outlier could be related to the observed slow leaks of the electrolyte that disrupts the electrochemical signal. Nevertheless, the similarly observed cell potentials between the in-situ and ex-situ tests suggest that we could use the cathodic potentials ex-situ collected to understand the cathode potential during the operando AFM test. A detailed discussion of the catalyst structural changes during ECO2R is provided in the following section.

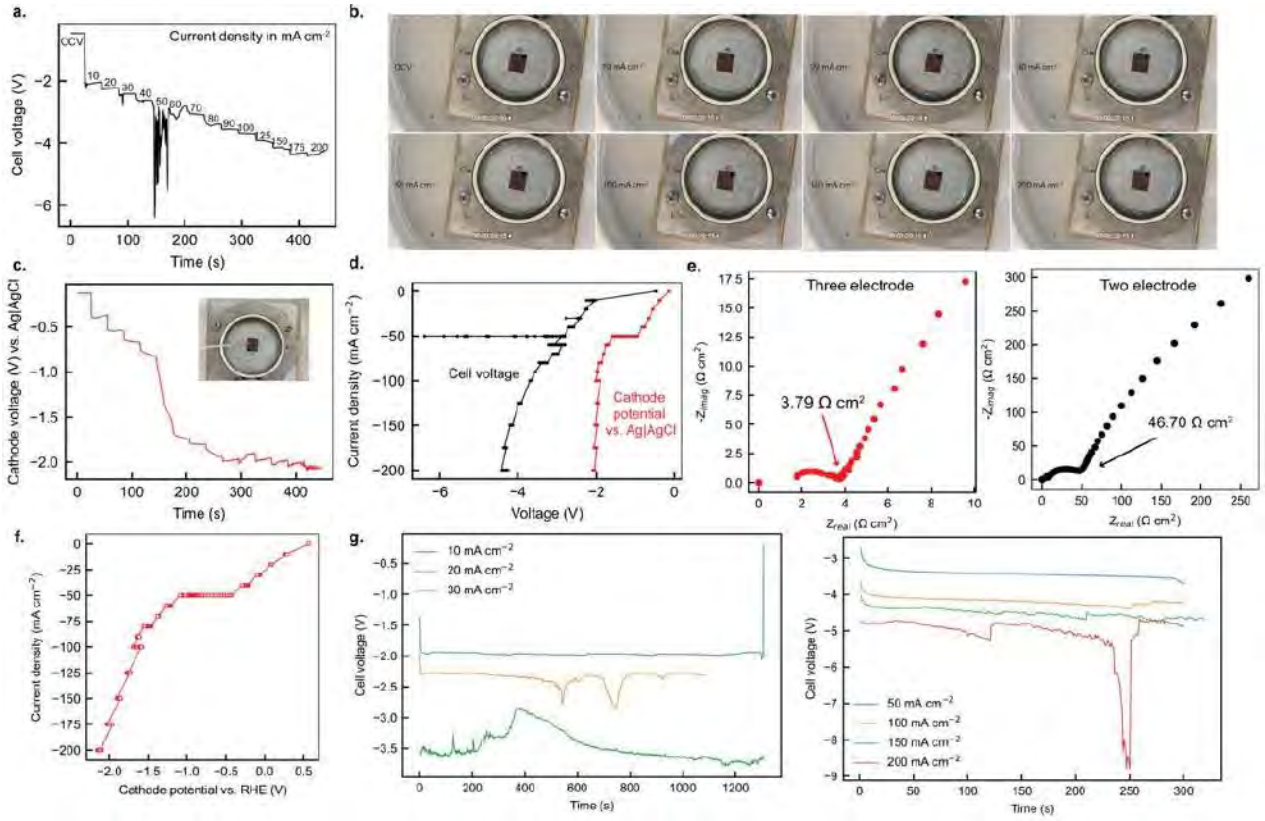

Figure 5: **a)** The applied cell potentials as a function of time under varied current densities. **b)** Selected frames of the recorded video of the cell during the chronopotentiometry analysis. **c)** The cathode potential vs. Ag|AgCl reference electrode of the GDE against time under varied current densities in the cell. The inset is a photo of the three-electrode testing configuration. **d)** Relations between current densities and applied cell or applied cathode potential vs. Ag|AgCl reference electrode. **e)** The electrochemical impedance spectra of the cell in the configuration of three-electrode (red) and two-electrode (black). **f)** The relation between the current densities and the calculated iR-corrected cathode potential vs. RHE. **g)** The chronopotentiometry curves of the cell during the EC-AFM characterization.

3.3 Catalyst layer structural change under ECO2R conditions

The AFM morphological images were recorded continuously for current densities lower than 30 mA cm^{-2}, with each scan taking 129 s. The size of the sample for the AFM measurement is 2×2 μm^2. **Figure 6**a shows the 3D topography image of the Cu catalyst layer as a function of time. Some images of a certain time, such as the image at 129 s for 10 mA cm^{-2}, are not presented in this report because these records experienced disruptions from the AFM tip. We found that the sample is slowly drifting during the operando test, which is likely due to the destabilization of the overall system conditions such as temperature and fluid motions. In this case, it is challenging to compare the AFM images directly. Alternatively, we cropped the location of the samples from the AFM images and studied their structural differences. They are noted in the red and blue frames in **Figure 6**a and highlighted in **Figure 6**b and c. Interestingly, there is no discernible change of catalyst structure in the operando AFM at 10 mA cm^{-2} ECO2R for at least 900 s. We acknowledge that the ECO2R duration plays a role in allowing the catalyst structural change observable in the AFM data.[10] However, the unavoidable sample drifting issue prevents us from investigating the exact location of the samples for more than 1000 s. Nevertheless, we could still conclude that the structural evolution is relatively slow at relatively low cathode potential.

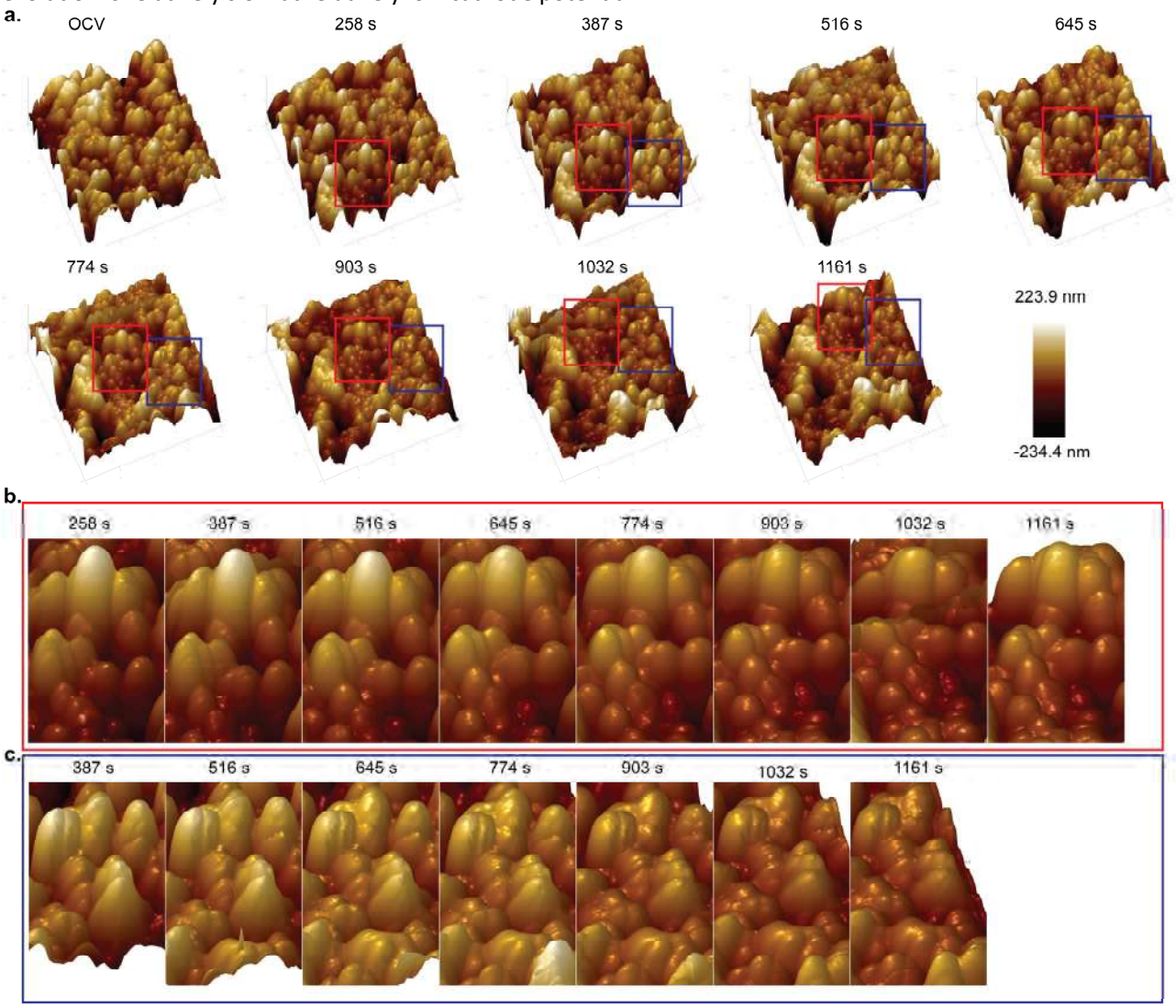

Figure 6 a) 3D AFM images of the Cu catalyst topography as a function of the duration of ECO2R at 10 mA cm^{-2}. The red and blue frames highlight the selected area of interest for comparison in **b)** and **c)**. The scale bar is only for the AFM image at 1161 s.

Similarly, we observed nearly no difference in the catalyst structures for the ECO2R operation at 20 mA cm^{-2} for at least 500 s, see **Figure 7**a, b and c. Additionally, we compared some selected peak force error images as shown in **Figure 7**d and e. The peak force error images recorded the tip peak force feedback and could provide detailed information of the surface texture but not the sample height information. Therefore, we could use the peak force error image to identify potential changes in the sample surface texture. Similarly, we observed no significant difference in the catalyst structure in the peak force error image.

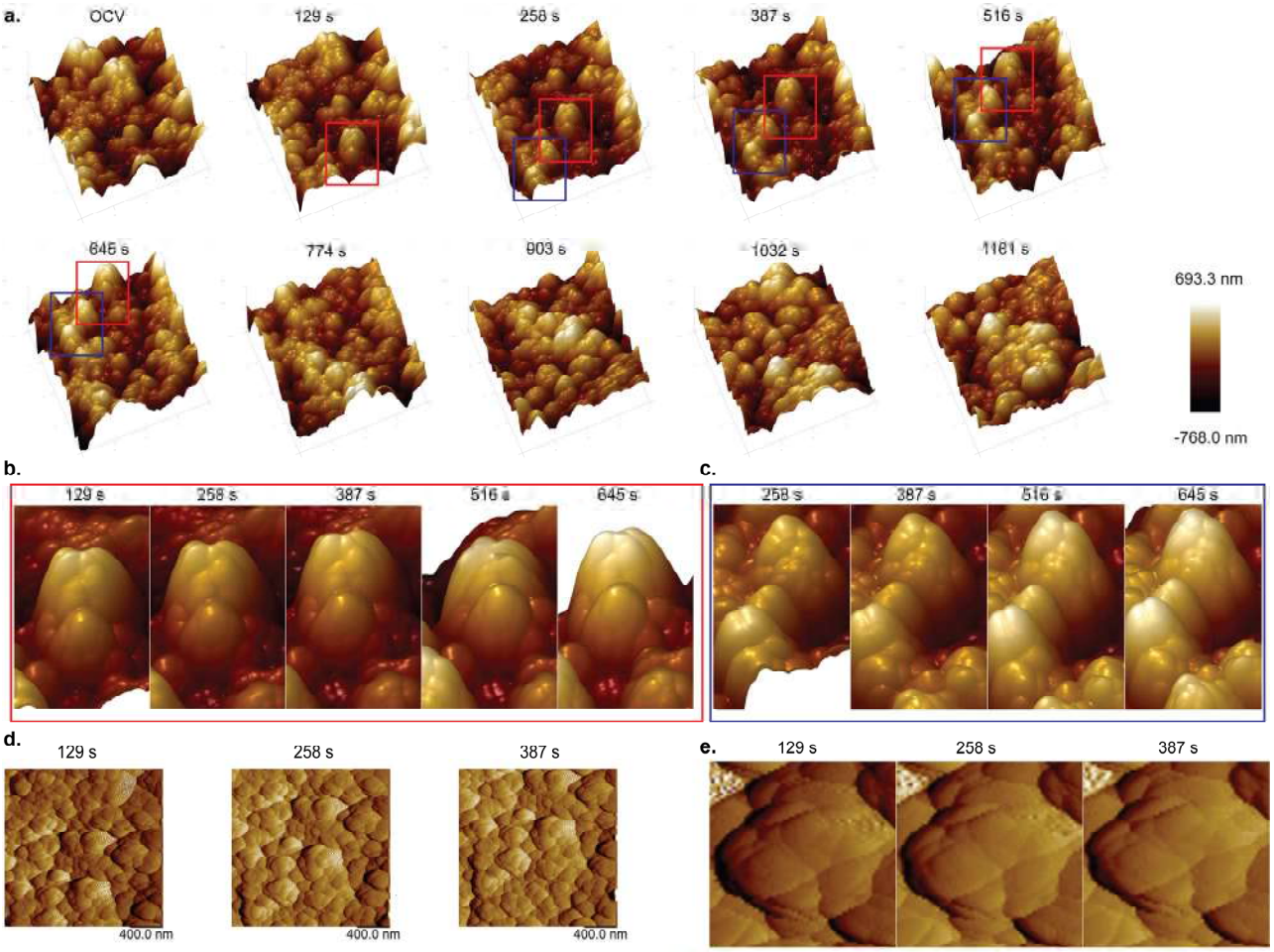

Figure 7: a) 3D AFM images of the Cu catalyst topography as a function of the duration of ECO2R at 20 mA cm^{-2}. The red and blue frames highlight the selected area of interest for comparison in **b)** and **c)**. The scale bar is only for the AFM image at 1161 s. Comparison of the peak force error images of **d)** the whole tested sample region and **e)** selected sample region at the exact location.

Because we did not observe a significant change of the sample structure at 20 mA cm^{-2}, we used the same sample to investigate the catalyst structure at 30 mA cm^{-2}. The 3D structural results are shown in **Figure 8**a, b, and c. We observed that the catalyst structure shows slightly more grain boundaries at 387 s and 516 s than the OCV in **Figure 8**b. A similar catalyst structure change was also observed at the selected AFM image at 1032 s and 1161 s compared to the one at 903 s. (see **Figure 8**c) Similar catalyst structural changes were also captured in **Figure 8**d and e, where more grain boundaries were formed at the catalyst surface during 30 mA cm^{-2} cathodic treatment. The formation of grain boundaries could be related to reducing the natural Cu oxide layer at the Cu catalyst surface.

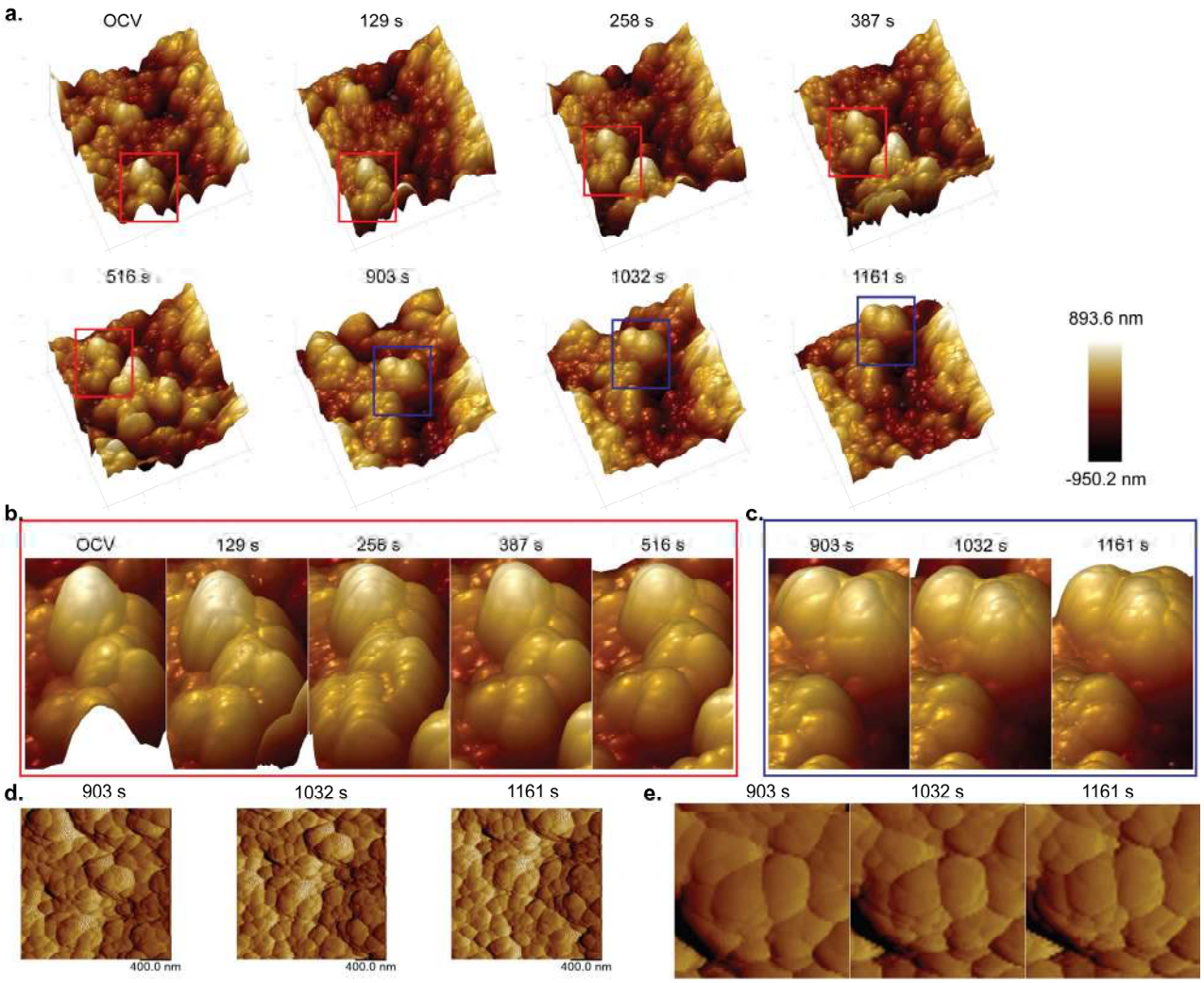

Figure 8: a) 3D AFM images of the Cu catalyst topography as a function of the duration of ECO2R at 30 mA cm^{-2}. The red and blue frames highlight the selected area of interest for comparison in **b)** and **c)**. The scale bar is only for the AFM image at 1161 s. Comparison of the peak force error images of **d)** the whole tested sample region and **e)** selected sample region at the exact location.

When the current densities are higher than 50 mA cm^{-2}, the EC-AFM tip was significantly disrupted and failed to deliver high-quality AFM images for the restructuring study. We addressed this critical issue by withdrawing the AFM tip before applying high current densities to the cell. After cathodic conditioning of the sample, we removed the formed bubbles and re-engaged the AFM tip to the sample surface. The 2D height images and peak force error images are compared in **Figure 9**. Although it is very challenging to locate the precisely same sample location, particularly for the microsize region, we successfully recorded two sets of the AFM images at nearly the exact locations: one is after 100 mA cm^{-2} conditioning, and the other one is after 150 mA cm^{-2}. We hence provided a detailed comparison of these two AFM images in **Figure 10**. In general, the high current densities (or more negative cathodic potential) led to a significant catalyst structural change. Notably, after 200 mA cm^{-2} conditioning for 30 s, we observed more nanocuboid structure (an indication of the formation of (100) facets) from the peak force error image. This finding is similar to the reports by Lee et al.[4] and Phan et al.[5] but at a much higher current density. Such difference scould be related to the much higher density of active sites in the catalyst layer in GDE than the ones at the planar electrode. The actual current density normalized by active surface area at 200 mA cm^{-2} over GDE might be of the same level over the planar electrode.

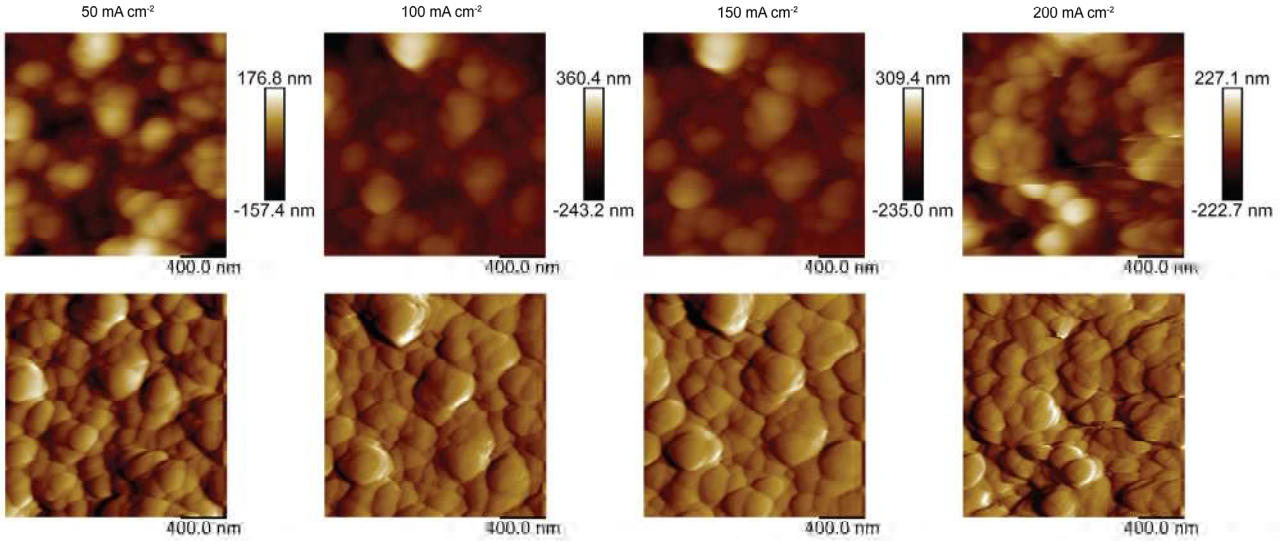

Figure 9: Summary of the 2D height sensor images (upper section) and peak force error images (bottom section) of the same sample after high current density conditioning for about 300 s each.

Figure 10a compares the 3D structures of the catalyst viewed from the top after 100 and 150 mA cm^{-2}. We could clearly see the change of the catalyst structure after 150 mA cm^{-2} conditioning. Notably, the change of the catalyst structure varies depending on the location. As shown in **Figure 10**b, more grain boundaries were formed at the places highlighted by red, green, dark blue, and purple circles. In contrast, some of the grain boundaries disappeared at the rest of the highlighted locations (i.e., by light blue and yellow circles) after 150 mA cm^{-2} conditioning. To further study the local structure change, we applied section analysis over the feature highlighted in red circles. To constrain the potential impacts from the different sample locations, we drew four lines over this feature on both AFM images (see **Figure 10**c) . We plotted the height data as a function of these locations (from top to bottom) in **Figure 10**d. This feature was flattened at the top and formed additional layers at the bottom after 150 mA cm^{-2}.

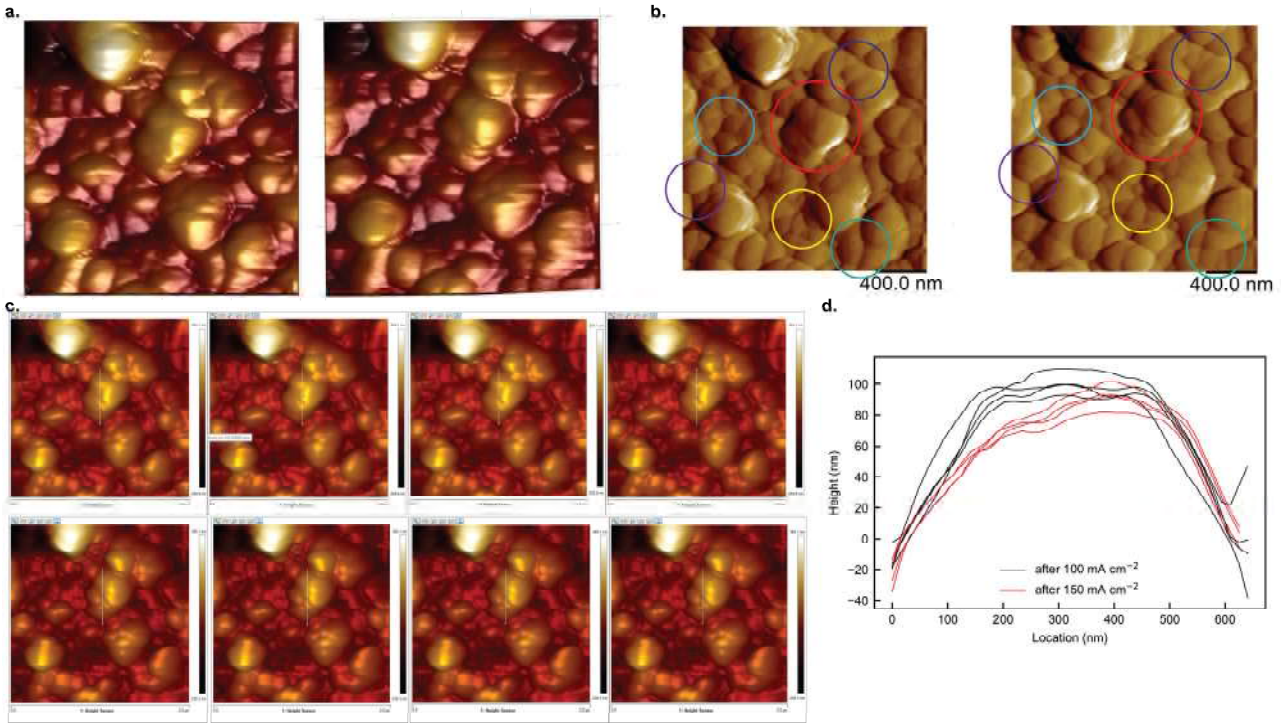

Figure 10: Comparison of **a)** top view of the 3D structure **b)** peak force error images of the catalyst after 100 mA cm^{-2} (left) and 150 mA cm^{-2} (right). The regions highlighted by the circles are regions with observable catalyst structural changes. **c)** Linear section analysis over the feature highlighted in the red circle in b) at the 3D structure images after 100 mA cm^{-2} (top section) and 150 mA cm^{-2} (bottom section) **d)** The corresponding height comparison over the feature analyzed in c).

3.4 Quantitative analysis of the surface restructuring

The EC-AFM images also provide the catalyst surface roughness and the actual surface area of the top surface of the catalyst layer. The averaged surface roughness can be quantified by the Rq and Ra parameters. The Rq is the root mean square average of height deviations, while Ra is the arithmetic average of the absolute values of the surface height deviations recorded from the mean image data plane. Note that the catalyst roughness is highly dependent on the sample locations, which can be exemplified by the considerable roughness difference between the samples treated for 10 mA cm^{-2} and 20-30 mA cm^{-2} shown in **Figure 11**a. Therefore, the sample drifting during the operando measurement has a profound impact on the recorded surface roughness. Nevertheless, we could still observe a general trend of the surface roughness at the catalyst layer from the data in **Figure 11**a.

In general, we found that the catalyst surface roughness increases with the conditioning duration under relatively low current densities such as below 30 mA cm^{-2}. The increase of the surface roughness could arise from the reduction of the natural Cu oxide layer, which leads to the formation of a rough surface. This roughness increase was only captured in the images for 30 mA cm^{-2} conditioning. Interestingly, the calculated surface roughness at high current densities slightly decreased when the catalyst was under high current densities, particularly when the size of the sample for AFM characterization is large (i.e., 10 $\times$10 and 5 $\times$ 5 um^2). We believed that the AFM data of the large sample area could reflect the general structural response of the catalyst to the applied potential. The reduced surface roughness is correlated with the flattened catalyst surface as observed from the peak force error images and section analysis for 100 and 150 mA cm^{-2} conditioning, as shown in **Figure 10**. The restructuring process occurs mainly from the dissolution of Cu ions in the electrolyte and re-electrodeposition process[3], where the applied potential provides the driving force for the Cu electrodeposition.

We also calculated the specific surface area by normalizing the actual catalyst top surface determined from the AFM images by the geometric electrode surface area exposed to the electrolyte (i.e., the size of the hole on the

tape, 0.07 cm^2). The results, as shown in **Figure 11**b, indicate the specific surface area remains similar for low current densities but slightly decreases at current densities higher than 50 mA cm^{-2}.

We also compared the specific current densities normalized by the actual surface area of the top surface of the catalyst. Although this parameter cannot truly reflect the specific current density normalized by the total active surface area, the trend of the parameter may be helpful to understand how the dynamic morphological change affects the local catalyst reactivity. As shown in **Figure 11**c, the sample drifting makes the specific current density vary significantly, particularly for the 30 mA cm^{-2}, indicating the local activity variations in the catalyst layer. Such local variations can also be shown in the study for the high current densities range, where the change of the tested sample size will affect the specific current densities.

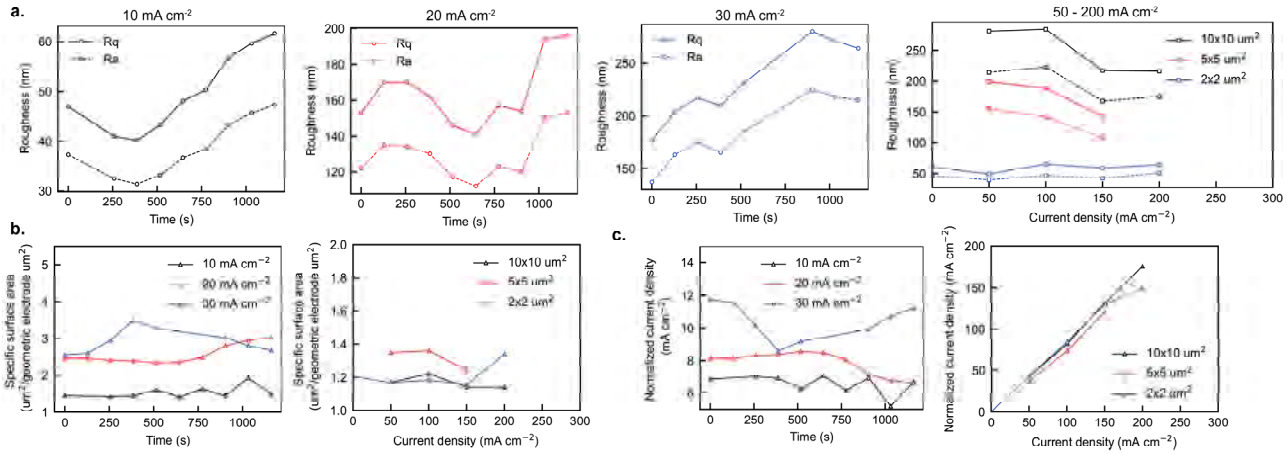

Figure 11: Comparison of **a)** the roughness Rq and Ra of the catalyst surface, **b)** specific catalyst top surface area, and **c)** specific current densities normalized by the actual top surface area calculated from the AFM images for different current-density studies.

3.5 The potential link between surface restructuring and ECO2R activity

The flow cell data discussed in Section 3.1 revealed that the ethylene faradaic efficiency increases rapidly at current densities between 50 and 200 mA cm^{-2}. Prior literature reported that ethylene production at Cu catalyst is generally favored at more negative cathode potentials, a high local pH[11] and CO concentration[12], oxide-derived Cu[11] or Cu with rough surface[11] or abundant (100) facets[13]. Increasing current density means an intensified cathode potential and induces high local pH. In our study, the reduction of the natural Cu oxide layer during ECO2R increases the cathode roughness, which could further contribute to a high local pH and exposure of low-coordinated atoms that are active for catalysis. This restructuring process likely contributes to the rapid increase of ethylene production at 50-200 mA cm^{-2}. However, the impact from the oxide-derivation in our case seems limited due to the limited Cu oxide at the surface, which can be evidenced by our recorded video and operando AFM images, which show that complete reduction of Cu only requires tens of minutes cathodic treatment at current densities below 50 mA cm^{-2}. After 200 mA cm^{-2} conditioning, we observed the formation of nanocuboids or Cu(100) facets at the catalyst surface. This facet could be favorable for ethylene production due to its high d-band center that binds strongly with intermediates and preferably stabilize the *CHO intermediate for ethylene production.[14] However, the ECO2R is a very complex process involving the catalyst structure and the electronic structure, local environment, transport phenomena, and operating conditions. Particularly at >200 mA cm^{-2}, the cathode performance could be limited by the local availability of CO_2 for the reaction, so the plateau of the ethylene faradaic efficiency at >200 mA cm^{-2} indicate that the formation of Cu (100) may not be the dominant factor affecting the activity of the catalyst.

4 CONCLUSIONS AND FUTURE WORK

This deliverable investigated the structural changes of the copper catalyst over a gas-diffusion electrode during the electrochemical CO_2 reduction at current densities between 10 mA cm^{-2} to 200 mA cm^{-2}. The EC-AFM results suggest no significant catalyst structure changes at < 30 mA cm^{-2} but discernable restructuring process > 30 mA cm^{-2}. The

restructuring process of the catalyst layer could take place via two consecutive stages: (1) the catalyst surface becomes rougher due to the reduction of the nature Cu oxide layer; (2) the catalyst layer is flattened along with the formation of the nanocuboid texture at > 50 mA cm^{-2}. Stage 1 likely contributes to promoting ethylene production, especially at below 100 mA cm^{-2}, via increasing local pH and providing under-coordinated atoms that are active for catalysis. The formation of nanocuboid texture in stage 2 is an indication of the formation of Cu (100) facets that could also benefit the ethylene conversion. However, the benign Cu (100) facets may not be the dominant factor determining the ECO2R reactivity above 200 mA cm^{-2} but maintaining an optimal local environment such as pH, CO_2, and CO availability likely plays an essential role. Additionally, our results also highlight the local variations of the catalyst morphology and activity, mainly arising from the non-uniformity of the as-prepared porous catalyst layer. Such local variations are expected to play a role in determining the overall cathode performance and stability for industrially relevant electrolysis.

The insights generated from this deliverable suggest that the conversion of CO_2 to ethylene could be promoted via (1) increasing catalyst surface roughness by amplifying the catalyst restructuring stage 1 such as oxide-derivation or introducing self-dissolution element (e.g., alkali metals ions) into the Cu lattice or (2) maximizing the catalyst electrochemically active surface area and transport of gas, ions, and electrons at high current densities by modifying the pore structure of catalyst layer and electrode wettability.

Future work following this deliverable will include further optimization of the EC-AFM cell to improve the liquid seal, optimization of the EC-AFM system to the in-situ characterization of CO_2 reduction products, and comprehensive studies of the roles of ionomers in the catalyst layer, electrolyte, cathodic treatment durations on the catalyst restructuring process. We expect these future studies to enable a better understanding of the catalyst structure-activity relationships, and the new insights could guide the design of the pre-catalysts towards a highly active and stable cathode for electrochemical CO_2 reduction.

5 REFERENCES

1. Kim, Y.-G.; Baricuatro, J. H.; Soriaga, M. P., Surface Reconstruction of Polycrystalline Cu Electrodes in Aqueous Khco3 Electrolyte at Potentials in the Early Stages of Co2 Reduction. *Electrocatalysis* **2018**, *9*, 526-530.
2. Arán-Ais, R. M.; Rizo, R.; Grosse, P.; Algara-Siller, G.; Dembélé, K.; Plodinec, M.; Lunkenbein, T.; Chee, S. W.; Cuenya, B. R., Imaging Electrochemically Synthesized Cu2o Cubes and Their Morphological Evolution under Conditions Relevant to Co2 Electroreduction. *Nature Communications* **2020**, *11*, 3489.
3. Huang, J.; Hörmann, N.; Oveisi, E.; Loiudice, A.; De Gregorio, G. L.; Andreussi, O.; Marzari, N.; Buonsanti, R., Potential-Induced Nanoclustering of Metallic Catalysts During Electrochemical Co2 Reduction. *Nature Communications* **2018**, *9*, 3117.
4. Lee, S. H., et al., Oxidation State and Surface Reconstruction of Cu under Co2 Reduction Conditions from in Situ X-Ray Characterization. *Journal of the American Chemical Society* **2021**, *143*, 588-592.
5. Phan, T. H.; Banjac, K.; Cometto, F. P.; Dattila, F.; García-Muelas, R.; Raaijman, S. J.; Ye, C.; Koper, M. T. M.; López, N.; Lingenfelder, M., Emergence of Potential-Controlled Cu-Nanocuboids and Graphene-Covered Cu-Nanocuboids under Operando Co2 Electroreduction. *Nano Letters* **2021**, *21*, 2059-2065.
6. Velasco-Velez, J.-J., et al., Revealing the Active Phase of Copper During the Electroreduction of Co2 in Aqueous Electrolyte by Correlating in Situ X-Ray Spectroscopy and in Situ Electron Microscopy. *ACS Energy Letters* **2020**, *5*, 2106-2111.
7. Vavra, J.; Shen, T.-H.; Stoian, D.; Tileli, V.; Buonsanti, R., Real-Time Monitoring Reveals Dissolution/Redeposition Mechanism in Copper Nanocatalysts During the Initial Stages of the Co2 Reduction Reaction. *Angewandte Chemie International Edition* **2021**, *60*, 1347-1354.

8. Nesbitt, N. T.; Smith, W. A., Operando Topography and Mechanical Property Mapping of Co2 Reduction Gas-Diffusion Electrodes Operating at High Current Densities. *Journal of The Electrochemical Society* **2021**, *168*, 044505.
9. Li, J., et al., Copper Adparticle Enabled Selective Electrosynthesis of N-Propanol. *Nature Communications* **2018**, *9*, 4614.
10. Grosse, P.; Gao, D.; Scholten, F.; Sinev, I.; Mistry, H.; Roldan Cuenya, B., Dynamic Changes in the Structure, Chemical State and Catalytic Selectivity of Cu Nanocubes During Co2 Electroreduction: Size and Support Effects. *Angewandte Chemie International Edition* **2018**, *57*, 6192-6197.
11. Mistry, H., et al., Highly Selective Plasma-Activated Copper Catalysts for Carbon Dioxide Reduction to Ethylene. *Nature Communications* **2016**, *7*, 12123.
12. Wicks, J., et al., 3d-Printable Fluoropolymer Gas Diffusion Layers for Co2 Electroreduction. *Advanced Materials* **2021**, *33*, 2003855.
13. Jiang, K.; Sandberg, R. B.; Akey, A. J.; Liu, X.; Bell, D. C.; Nørskov, J. K.; Chan, K.; Wang, H., Metal Ion Cycling of Cu Foil for Selective C–C Coupling in Electrochemical Co2 Reduction. *Nature Catalysis* **2018**, *1*, 111-119.
14. Luo, W.; Nie, X.; Janik, M. J.; Asthagiri, A., Facet Dependence of Co2 Reduction Paths on Cu Electrodes. *ACS Catalysis* **2016**, *6*, 219-229.